

Rapid Determination of Translational Diffusion Coefficients Using ESR Imaging*

D. A. CLEARY, Y.-K. SHIN, D. J. SCHNEIDER, AND J. H. FREED

Baker Laboratory of Chemistry, Cornell University, Ithaca, New York 14853

Received October 26, 1987; revised January 8, 1988

The use of ESR imaging for the rapid determination of diffusion coefficients, D , in anisotropic solvents is reported, and the use of Fourier transforms of the concentration profile to determine D is discussed. An approximate rapid analysis technique is also presented. The diffusion coefficients for motion perpendicular to the director axis for 4-oxo-2,2,6,6-tetramethylpiperidine-1-oxyl (TEMPONE) and octylbenzoyl spin label (OBSL) in the nematic phase of Phase V have been determined. They are $D(\text{TEMPONE}) = 1.25 \times 10^{-7} \text{ cm}^2 \text{ s}^{-1}$ and $D(\text{OBSL}) = 0.48 \times 10^{-7} \text{ cm}^2 \text{ s}^{-1}$ at 294 K. The lateral diffusion coefficients for cholestane spin label (CSL) in POPC and 16PC in DMPC were also determined. The diffusion coefficients were measured as a function of temperature from 11 to 60°C and they range from 4×10^{-8} to $2 \times 10^{-7} \text{ cm}^2 \text{ s}^{-1}$. Activation energies for diffusion in the two systems are $E_a(\text{CSL/POPC}) = 6.30 \text{ kcal mol}^{-1}$ and $E_a(16\text{PC/DMPC}) = 8.63 \text{ kcal mol}^{-1}$. © 1988 Academic Press, Inc.

INTRODUCTION

ESR imaging is currently enjoying an active growth period. Most of the work to date on ESR imaging has involved static samples (1-5). The use of "dynamic samples" to investigate transport phenomena has been accomplished in a few instances (6-9). We use the term dynamic sample to describe a sample with an inhomogeneous distribution of spin probes dissolved in a fluid solvent. With the passage of time, this inhomogeneous distribution will tend to a homogeneous distribution via translational diffusion. All these experiments to measure diffusion coefficients required either long experimental times (6, 7, 9) (several days) or assumed an idealized distribution of the spin-probe concentration profile (8).

In our previous paper, we described an ESR imaging method for accurately determining the macroscopic translational diffusion coefficients of ESR spin probes dissolved in various isotropic and anisotropic solvents (7). As pointed out in that work, a major drawback of the experiments was the long experimental times required for a single measurement of the diffusion coefficient D , e.g., 5-7 days for $D \approx 10^{-7} \text{ cm}^2 \text{ s}^{-1}$. A more rapid method is desirable for several reasons: the effects of long-term instrumental instabilities are avoided, smaller diffusion coefficients become accessible to the measurement, and the temperature dependence of the diffusion coefficient

* Supported by NIH Grant GM25862 and NSF Grants DMR-86-04200 and CHE 87-03014.

can more conveniently and accurately be determined. In this paper we report on progress on our ESR imaging method that has resulted in a decrease (by at least four orders of magnitude) in the time required to accurately determine D , extended the minimum D that can *readily* be measured to at least as small as 10^{-8} cm² s⁻¹, and allowed for an arbitrary initial distribution of spin probes. The success of this work has resulted from two advances. First, the preparation of a highly localized distribution of spin probes within the solvent means that only a small increment of time is required for the concentration profile to change significantly, provided sufficient magnetic field gradients are utilized. This also has the benefit of avoiding corrections for spectrometer sensitivity variations (7). Second, an analysis in Fourier space overcomes many of the problems associated with accurately determining concentration profiles in real space. We report here on the rapid determination of D (perpendicular) for spin probes in the nematic liquid crystal Phase V at room temperature, and we present initial results on lateral diffusion coefficients in phospholipids. These include the lateral diffusion coefficients of 16PC in DMPC and of CSL in POPC at various temperatures and the associated activation energies.

EXPERIMENTAL

Instrumental. All ESR experiments reported here were performed at X band on a Varian Model E12 spectrometer. The spectra were recorded in the first derivative mode with 100 kHz field modulation and microwave powers of about 5 mW. The modulation amplitude was set to 20% of that required for maximum signal. Because a resonance line in the presence of a magnetic field gradient is broader than that in the absence of any gradients, larger modulation amplitudes were used in the gradient-on spectra than in the gradient-off spectra to maintain the 20% rule. Failure to observe this condition led to difficulties in the subsequent analysis. That is, when the same modulation amplitude was used for both the gradient-on and the gradient-off spectra, the deconvolution did not result in an acceptable one-dimensional image of the concentration profile. Instead, the profile was corrupted with noise of all frequencies to the point that the image of the concentration profile was lost. We do not, as yet, have a complete explanation for this observation.

In order to record ESR images, a linear magnetic field gradient superimposed on the main static magnetic field is necessary. In the experiments described here, that gradient is perpendicular to the direction of the static field. The gradient was produced two different ways, depending on the magnitude required for the two different systems (liquid crystal and phospholipid). A pair of figure-eight coils previously described was used in the phospholipid experiments (7). These coils produced a gradient of 36 G/cm at a current of 1.5 A. For the liquid-crystal experiments, a pair of matched ferromagnetic wedges, machined from 1018 cold rolled steel, produced a gradient of 282 G/cm. Temperature control and variation were accomplished in the phospholipid experiments by using an 11 mm o.d. single wall Dewar and a nitrogen flow system, with a standard Varian temperature control unit. All the liquid-crystal experiments were performed at room temperature with no regulation. Experimental times were short enough (1 h) such that the temperature remained constant. Data were collected on a Leading Edge Model D PC interfaced to an HP 3457 multimeter. The multimeter monitored the analog signal going to the XY recorder of the ESR

spectrometer. All spectra were digitized to 1024 points, had 100 G sweep widths, and had 1 min sweep times. In the phospholipid experiments, a gradient-on and a gradient-off spectrum were recorded for each time t . This was possible because the current in the gradient coils could simply be turned on or off as needed. In the liquid-crystal experiments, gradient-on spectra were continuously recorded until the experiment was over. At that time, the wedges were removed and a single gradient-off spectrum was recorded.

In these experiments it was possible to neglect the variation of cavity sensitivity with position (7), because of the narrow initial distribution of spin probe (0.1–1.0 mm). If this distribution is centered in the cavity, the sensitivity variation is less than 5% across the sample during the course of the experiment.

The nematic liquid crystal, Phase V, aligns in the static magnetic field with the director axis parallel to the field. The diffusion of spin probe that is observed in this arrangement is perpendicular to the director axis, and hence the diffusion coefficients reported are perpendicular diffusion coefficients D_{\perp} .

Preparation of liquid-crystal sample. One of the requirements for rapid determination of diffusion coefficients is that the initial distribution of diffusing spin probes be confined to a narrow region within the solvent. Therefore, the following procedure was adopted. A 5 mm o.d. (4.5 mm i.d.) NMR flat bottom tube (Norell) made from borosilicate glass and flat on both the inside and the outside was used as a sample tube. Approximately 3 μ l of a 0.001 M solution of TEMPONE in the nematic liquid crystal Phase V was deposited on the bottom of the NMR tube. The bottom of the tube was pressed against dry ice to freeze this layer of solution, approximately 0.8 ml of pure Phase V was added, and the tube was then allowed to warm to room temperature. This procedure resulted in a TEMPONE solution of Phase V where the TEMPONE initially occupied the bottom 10% region of a 5 mm high solution. After the sample came to room temperature, it was placed in a Varian TE₁₀₂ cavity and positioned such that the bottom of the sample tube was centered in the cavity. Data collection began immediately with approximately 90 s between scans. Normally, 30 scans were adequate to determine D (perpendicular) to within 10% precision. The diffusion coefficient of octylbenzoyl spin label (OBSL) in Phase V was determined using an identical preparation technique.

Preparation of phospholipid. 1,2-Dimyristoyl-*sn*-glycero-3-phosphatidylcholine (DMPC) and 1-palmitoyl-2-oleoyl-*sn*-glycero-3-phosphatidylcholine (POPC) were purchased from Avanti Polar Lipid, Inc., and used without further purification. The 3-doxyl derivative of cholestan-3-one (CSL) was obtained from Syvar, and 1-palmitoyl-2-(16-doxyl stearoyl) phosphatidylcholine (16PC) probe was a gift from Professor G. W. Feigenson, Department of Biochemistry, Cornell University, who synthesized it according to standard methods (10).

One of the basic sample requirements in these experiments is to have the spin probe initially localized near the center of the plates in a thin strip perpendicular to the direction of the magnetic field gradient (see Fig. 1), so that one does not have to be concerned about reflecting wall boundary conditions in the analysis. The following procedure for preparing the sample was adopted for that purpose. After the pure lipid solution (10 mg of lipid/ml chloroform) was prepared, the desired spin probe was added to a small portion of the solution to achieve 0.75 mol% spin-probe concentra-

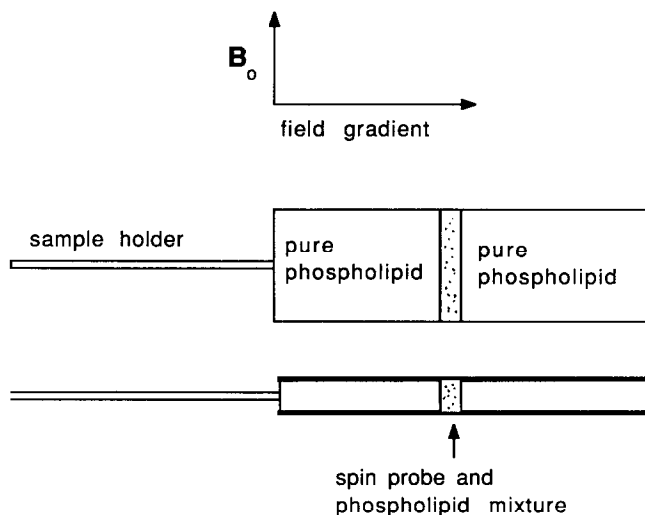


FIG. 1. Sample configuration for determination of fast lateral diffusion coefficients in phospholipid. Figure is not to scale. The initial distribution is shown as a square shape, but in fact is Gaussian (see text).

tion with respect to the pure lipid. Approximately 700 ml of the pure lipid solution was removed and the solvent was evaporated by blowing dry nitrogen to concentrate the lipid 10-fold. The concentrated lipid solution was spread evenly with a 100 μ l syringe on one of the two clean glass plates (8 \times 22 cm², Corning No. 1 slide glass, Corning, New York). Next, 50 μ l of spin-probe-phospholipid mixture solution was dried in the same way and delivered with a 10 μ l syringe onto the second glass plate to make a thin strip of the spin-probe-phospholipid mixture along the center of the glass plate. After that, the two plates were placed in a high-humidity nitrogen flow apparatus to hydrate the lipid and further evaporate the solvent. The temperature of the apparatus was kept at 45°C with a Haake water bath-circulator. When the solvent was fully evaporated, the plates were taken from the assembly, and the midsection of the pure lipid on the first plate was cut out by a razor blade to accommodate the spin-probe-phospholipid mixture strip on the second plate when the two plates were put together to make a sandwich (see Fig. 1). The strip of spin-probe-phospholipid mixture on the second plate was also trimmed to be approximately 0.5 mm wide. To make sure that the solvent has evaporated completely, both plates were placed under vacuum (\approx 0.2 mm Hg) for 1 day. The lipid plates were then rehydrated by the same technique described above. After rehydration, the plates were put together and aligned, by procedures essentially the same as those of Tanaka and Freed (11). For details on these procedures and characterization methods for the ordered samples see Ref. (11). The water content of the sample was determined by weighing the sample after the ESR measurement, before and after evacuation for 3 days at 0.002 mm Hg. The DMPC sample was found to have 10–15% water by weight.

ANALYSIS

Spectra recorded in the presence of a magnetic field gradient, $I_g(H)$, are a convolution of two functions,

$$I_g(H, t) = \int_{-\infty}^{+\infty} I_0(H')C(H - H', t)dH', \quad [1]$$

where $I_0(H)$ is the spectrum in the absence of any gradients and $C(H)$ is the distribution of spin probes along the magnetic field gradient. To convert $C(H)$ to $C(x)$, the one-dimensional concentration profile in units of cm^{-1} , the conversion factor B' is used,

$$C(B'x, t) = C(H, t), \quad [2]$$

where B' is the magnitude of the magnetic field gradient in units of G/cm. The value of B' was determined from an independent measurement by translating a point sample of DPPH a known distance and recording the shift in its resonance line position.

The determination of $C(B'x, t) = C(H, t)$ from the two recorded spectra $I_g(H, t)$ and $I_0(H)$ is, in principle, a straightforward calculation. If the Fourier transforms of the two spectra are represented as

$$I_g(k, t) = \text{FT}[I_g(H, t)] \quad [3]$$

$$I_0(k) = \text{FT}[I_0(H)] \quad [4]$$

then $C(B'x, t)$ is equal to (12)

$$C(B'x, t) = \text{FT}^{-1} \frac{I_g(k, t)W(k)}{I_0(k)}, \quad [5]$$

where FT^{-1} means inverse Fourier transform. $W(k)$ is a modified Wiener filter function that is necessary to accomplish the indicated division and also suppresses noise. It has the form

$$W(k) = \frac{|I_g(k, t)|^2}{|I_g(k, t)|^2 + u}. \quad [6]$$

The variable k (G^{-1}) is used for the reciprocal space of H (G). The constant u is of the order of the unit round-off error. Without the filter function, numerical overflow problems occur when the denominator approaches zero (7). An analysis that depends on $C(B'x)$ will suffer from the accumulated errors of two forward Fourier transforms, one filtered division, and one back Fourier transform.

The final back transform step and the use of the filter function can be avoided as follows.

The Fourier transform of the one-dimensional concentration profile is

$$C(k) = \frac{I_g(k)}{I_0(k)}. \quad [7]$$

The constant B' can be ignored until the last step of the analysis [so D initially is in units of $\text{G}^2 \text{s}^{-1}$], when division by B'^2 gives D in the correct units of $\text{cm}^2 \text{s}^{-1}$.

The concentration of spin probe is kept low to avoid Heisenberg spin-exchange effects and to render Fick's second law valid (13):

$$\frac{dC(x, t)}{dt} = D \frac{d^2C(x, t)}{dx^2}. \quad [8]$$

For an arbitrary initial distribution of spin probes, $C(x, 0)$ (neglecting for the moment any boundary effects), one may first write down the Green's function and thus obtain the solution

$$C(x, t) = 1/\sqrt{4\pi Dt} \int_{-\infty}^{+\infty} \exp(-(x-x')^2/4Dt)C(x', 0)dx' \quad [9]$$

which is just a convolution of the Green's function with the initial distribution (14, 15). Taking the Fourier transform of both sides, one obtains

$$C(k, t_1) = \exp(-k^2 D(t_1 - t_0))C(k, t_0) \quad [10]$$

or alternatively,

$$\ln C(k, t_1) = -k^2 D(t_1 - t_0) + \ln C(k, t_0). \quad [11]$$

For the purposes of plotting and obtaining a slope, the $C(k, t_j)$, which are complex, may be written in polar form,

$$C(k, t_1) = R_1 \exp(i\phi_1) \quad [12]$$

$$C(k, t_0) = R_0 \exp(i\phi_0) \quad [13]$$

with $R_j = |C(k, t_j)|$ and $\phi_j = \phi_j(k)$. Equation [11] can then be expressed as

$$\ln R_1 + i\phi_1 = -k^2 D(t_1 - t_0) + \ln R_0 + i\phi_0. \quad [14]$$

Equating the real parts and neglecting the imaginary parts results in

$$\ln R_1 - \ln R_0 = -k^2 D(t_1 - t_0) \quad [15]$$

which involves only real numbers. [Note that $I_0(k)$ cancels in Eqs. [11] and [15] when Eq. [7] is substituted. This is a consequence of the absence of boundaries (cf. below).]

Combining Eqs. [15] and [7] leads to a convenient algorithm for calculating D , given $C(k, t)$ for at least two times, t_0 and t_1 . This algorithm is further simplified by the absence of the filter function in Eq. [7]. This does not result in numerical overflow problems when the range of k values is restricted to the first ≈ 100 k values of a total of 1024. The appropriateness of this restriction will be demonstrated presently. Equation [15] can be plotted in several ways to obtain D . Although formally equivalent, the different methods result in different levels of precision because of the relative magnitudes of the slope and the intercept for each case.

One approach to plotting Eq. [15] is to plot for a given k the time dependence of the $C(k, t)$. This should give a straight line with the slope of $-k^2 D$. A second plot of these $k^2 D$ values versus k^2 results in the value of D . When fitting Eq. [15] in such a manner, both the slope ($-k^2 D$) and the intercept [$\ln R_0(k)$] are being determined simultaneously. However, the value of the intercept is several orders of magnitude larger than the slope and this resulted in considerable scatter in trying to determine the value of $-k^2 D$.

A second approach to plotting Eq. [15] is to pair the data for n times into $n/2$ pairs (16). Then for one such pair, t_1 and t_0 , plot $\ln |C(k, t_1)| - \ln |C(k, t_0)|$ versus k^2 :

$$\ln |C(k, t_1)| - \ln |C(k, t_0)| = -k^2 D(t_1 - t_0). \quad [16]$$

The slope equals $-D(t_1 - t_0)$. The slopes from each pair of data sets are then plotted

versus Δt values resulting in D . It is most useful to take as pairs from the set $C(k, t_i)$, where $i = 1 \dots n_1; t_n - t_1, t_{n-1} - t_2, \dots, t_{n/2+1} - t_{n/2}$.

Both approaches result in the same value of D ; however, the second approach had a much smaller standard deviation for D , since the effects of the large intercept are first removed. The two approaches to plotting the $C(k, t_j)$ are best seen when the values of k are assembled as a matrix. The $C(k)$ values for a given t_i are written as a row vector. Each successive row is an increment in time:

$$\begin{array}{c}
 t/k \\
 0 \\
 1 \\
 2 \\
 3 \\
 \vdots \\
 30
 \end{array}
 \begin{bmatrix}
 1 & 2 & 3 & \dots & 1024 \\
 k_1 & k_2 & k_3 & \dots & k_{1024} \\
 k_1 & k_2 & k_3 & \dots & k_{1024} \\
 k_1 & k_2 & k_3 & \dots & k_{1024} \\
 k_1 & k_2 & k_3 & \dots & k_{1024} \\
 \vdots & \vdots & \vdots & \ddots & \vdots \\
 k_1 & k_2 & k_3 & \dots & k_{1024}
 \end{bmatrix}
 .$$

The first approach involves plots down a column as a function of t . The second approach involves subtracting one row from a second one ($t_1 - t_0$, for example) and then plotting the resulting differences as a function of k^2 .

Equation [11] is modified slightly when a reflecting wall boundary condition is imposed, as for the liquid-crystal samples where a flat bottom sample tube is used:

$$\ln\{\text{Real}\{C(k, t_1)\}\} = -k^2 D(t_1 - t_0) + \ln\{\text{Real}\{C(k, t_0)\}\}. \tag{17}$$

This is a result of the fact that at the reflecting wall

$$\frac{\partial C(x)}{\partial x} = 0 \quad \text{at } x = 0 \tag{18}$$

which is obeyed by $\cos(kx)$ but not by $\sin(kx)$. In the phospholipid experiment, no boundary conditions are imposed, and therefore the full Fourier transform is used as implied in Eq. [15]. When Eq. [17] is used, it is important that the sample be placed in the cavity such that the centers of the gradient-on and gradient-off spectra [i.e., $I_g(H)$ and $I_0(H)$, respectively] coincide. If they do not, a k -dependent phase factor is required in Eq. [17] to correct for the offset. In x space, this alignment corresponds to the maximum of $C(x, t)$ being at $x = 0$. Our experience suggests that the effort required for proper alignment of the sample is preferred over use of the phase factor.

Regardless of whether Eq. [15] or [17] is applicable, only a finite number of k values are useful for any reasonable $(t_1 - t_0)$, because the (natural) log of $C(k)$ is used in the calculations. After the ≈ 100 th k value, the magnitude of $C(k)$ is on the order of the unit round-off error for single precision modeling calculations, and this is, of course, much better signal-to-noise than in actual experiments. When these small numbers are the argument of the natural log, spurious values for $\ln[C(k, t)]$ are obtained. Figure 2 is a simulation which shows two Gaussian concentration distribution profiles where $D = 10^{-7} \text{ cm}^2 \text{ s}^{-1}$ and $(t_1 - t_0) = 10^3 \text{ s}$. A plot of Eq. [15] for these two concentration profiles is shown in Fig. 3. Only about 30 k values are useful in this case. The corruption of the remaining k values is due to the limited precision of the computer. All of the calculations in this work were done in single precision. Thus, a simple check to find the maximum possible k value involves the following: from Eq. [5], the FWHM of a $C(x, t_0)$ and a $C(x, t_1)$ for $t_1 \neq t_0$ is determined approximately. These FWHM

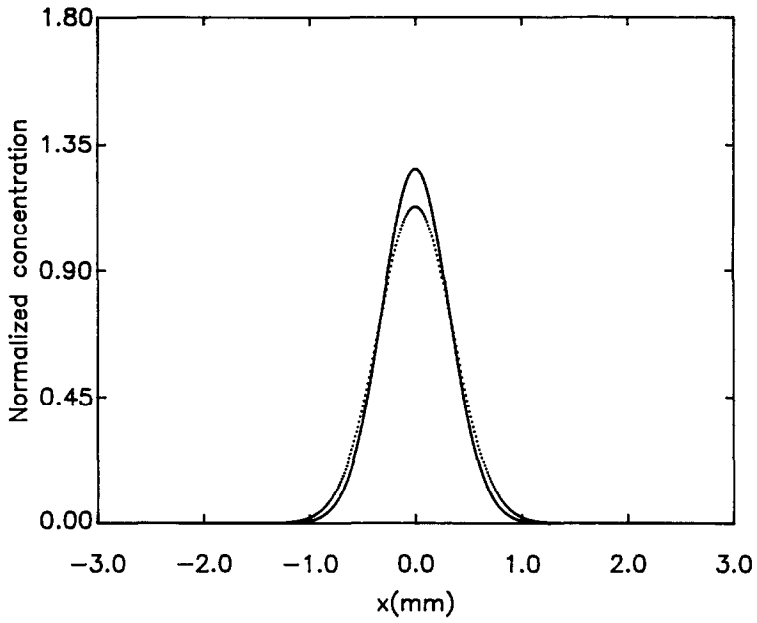


FIG. 2. Two Gaussian concentration profiles at time t_0 and at a later time, t_1 ($D = 10^{-7} \text{ cm}^2 \text{ s}^{-1}$, $t_1 - t_0 = t = 10^3 \text{ s}$). For each Gaussian, 512 points were created and each curve was Fourier transformed to 1024 points by zero-filling.

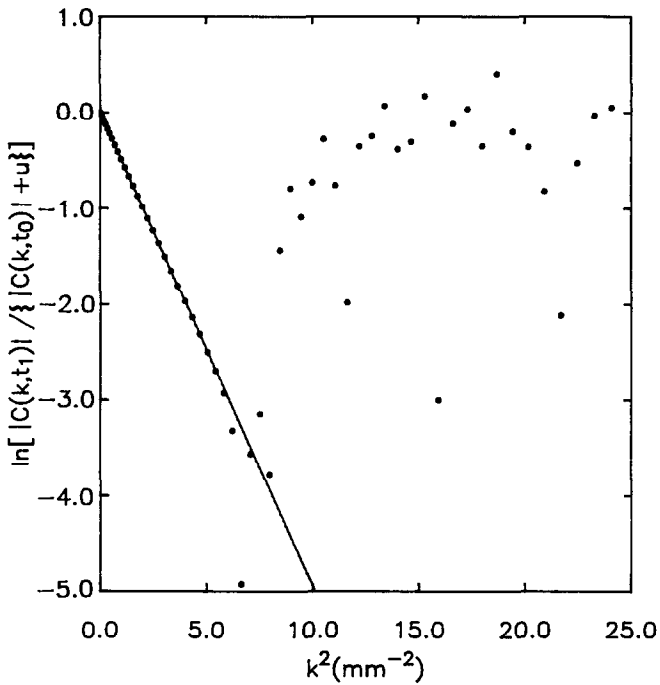


FIG. 3. A plot of $\ln\{ |C(k, t_1)| / \{ |C(k, t_0)| + u \} \}$ versus k for the two Gaussians shown in Fig. 2. Note that only the first 30 values of k are useful.

values are used to model the two $C(x, t)$ with Gaussians, and the two Gaussians are Fourier transformed. The quantity $\ln[|C(k, t_1)|/\{|C(k, t_0)| + u\}]$ is then plotted vs k^2 , where u is of the order of the machine precision ($\approx 10^{-15}$). The plot is linear up to the maximum possible k , then the points abruptly become randomly scattered. The maximum value of k obtained in this way is higher than can be achieved in an experiment, due to the presence of experimental noise (17).

A quick method to determine D requires that the $C(k, t)$ be back transformed to $C(x, t)$. The maximum value of $C(x, t)$, which occurs at $x = 0$, is then plotted versus $1/(t + t_0)^{1/2}$. The adjustable parameter t_0 is the time required for a delta function initial distribution to evolve into the Gaussian distribution assumed to be present at the beginning of the experiment. Typically t_0 was of the order of 1200 s for our samples. This approach is based upon the fundamental solution of Fick's second law for an initial delta function distribution (12),

$$C(x, t) = \exp(-x^2/4Dt)/(4\pi Dt)^{1/2} \quad [19]$$

so that at $x = 0$,

$$C(x = 0, t) = 1/\sqrt{4\pi Dt}. \quad [20]$$

We found that the value of D obtained in this manner is within the experimental limits of the Fourier method, but its precision is much poorer. It does require the use of an adjustable parameter, t_0 , which is not required in the Fourier analysis. Finally, the accuracy is severely limited by the need for the Wiener filter (cf. Eq. [5]).

RESULTS

The first 10 spectra recorded immediately after the TEMPONE/liquid-crystal sample reached room temperature are shown in Fig. 4. The sweep width was 100 G and

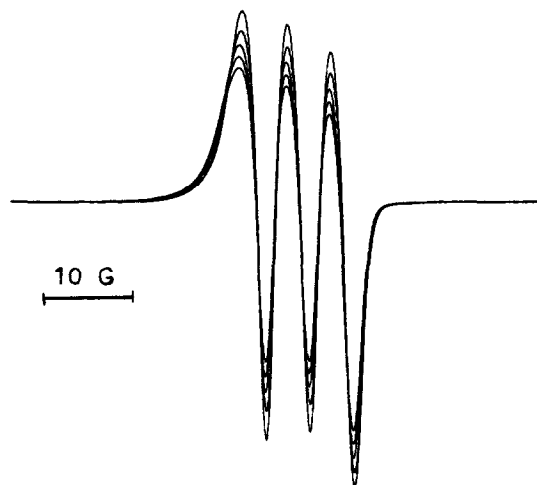


FIG. 4. A series of spectra from imaging concentration profiles along the X axis of the TE_{102} cavity. A sweep width of 100 G and sweep time of 1 min were used. The magnetic field gradient, provided by ferromagnetic wedges, was 282 G/cm. The diffusing spin probe is TEMPONE dissolved in Phase V. The spectra are approximately 180 s apart.

a scan time of 1 min was used. The delay between successive spectra results from the time required to dump the data (1024) points to the floppy disc on the PC. It is clear from such a collection of spectra that the concentration profile is changing rapidly with time. The rapid change in the profile (despite the slow diffusion, $D \approx 10^{-7} \text{ cm}^2 \text{ s}^{-1}$) is the result of the narrow initial distribution of spin probes combined with the substantial field gradient produced by the wedges.

A representative plot of Eq. [17] for two of the spectra shown in Fig. 4 is shown in Fig. 5. Equation [17] plotted for a pair of transformed concentration profiles for OBSL in Phase V is shown in Fig. 6. A plot of $D(t_1 - t_0)$ is shown in Fig. 7 for the TEMPONE case. Sixteen pairs of $C(k, t_i)$ were used in this plot. In Fig. 8 $D(t_1 - t_0)$ is plotted versus $(t_1 - t_0)$ for OBSL diffusion in Phase V. Only five pairs of $C(k, t_i)$ were used in this case. The diffusion coefficients obtained from plots such as those in Fig. 7 and Fig. 8 are given in Table 1.

If the one-dimensional concentration profile, $C(x)$, is Gaussian, then $C(k)$ will also be Gaussian and vice versa. If $C(k)$ is Gaussian, then a plot of $\ln |C(k)|$ versus k^2 will be linear. [Recall that Eq. [7] provides a straightforward method to calculate $C(k)$ without ever calculating $C(x)$.] We have found from imaging the initial $C(x)$ that the Gaussian assumption is valid for the phospholipid samples. Thus, in the analysis of the phospholipid data, we found it more convenient to simply plot $\ln |C(k, t_i)|$ versus k^2 , and then plot the resulting slopes versus t_i to obtain D . That is, for a Gaussian distribution in x of width δ at $t = 0$ we have at time t

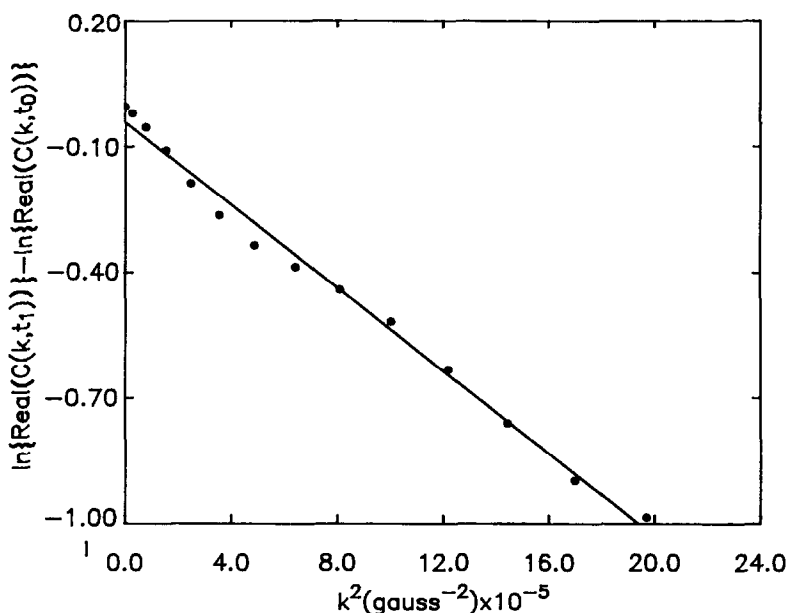


FIG. 5. A plot of $\ln\{\text{Real}\{C(k, t_1)\}\} - \ln\{\text{Real}\{C(k, t_0)\}\}$ versus k^2 (see Eq. [17] in text) for TEMPONE diffusing in Phase V. The slope of the line is equal to $-4\pi^2 D(t_1 - t_0)$. For each pair of times t_1 and t_0 , a plot like this is generated.

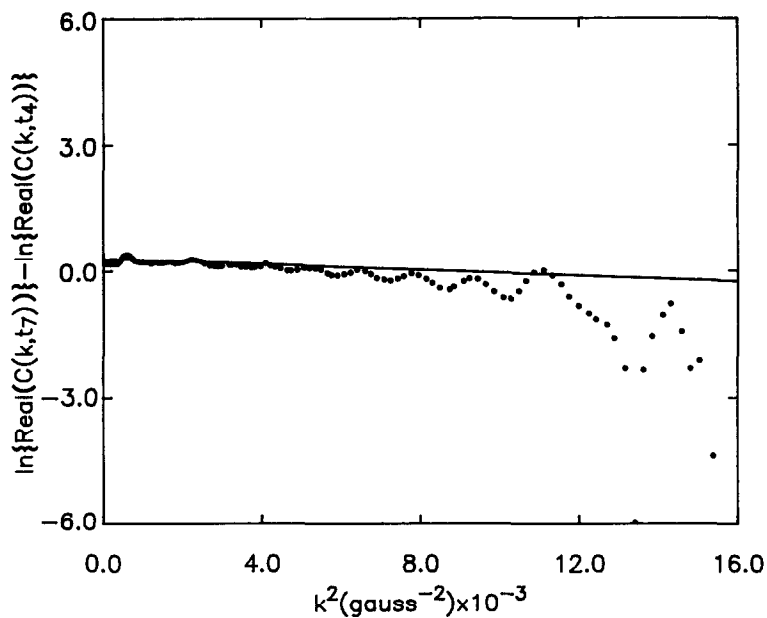


FIG. 6. Same type of plot as Fig. 5 except that the diffusing species is OBSL.

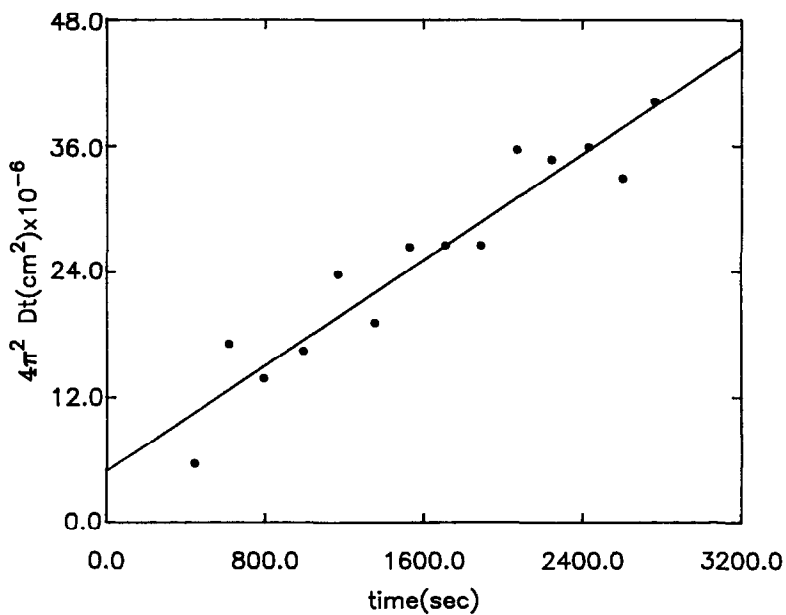


FIG. 7. A plot of $4\pi^2 Dt$ versus t [where $t = (t_1 - t_0)$] for TEMPONE in Phase V.

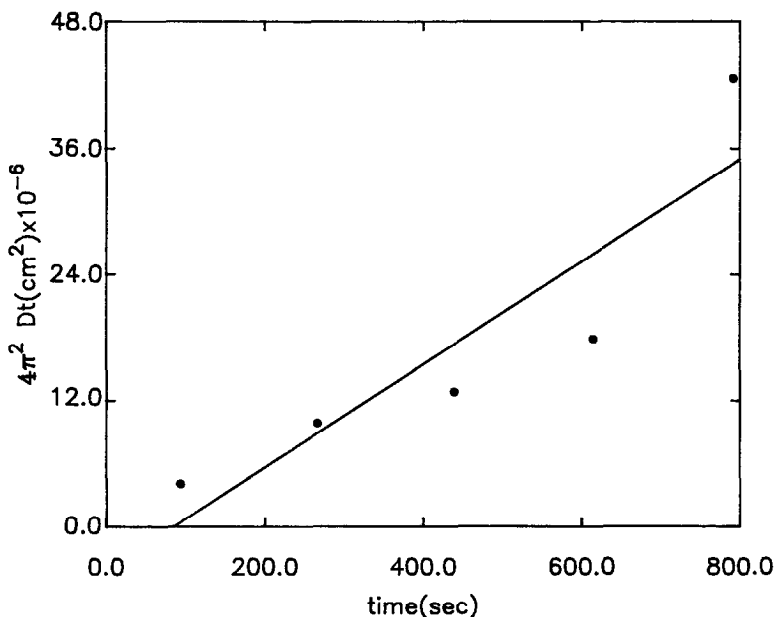


FIG. 8. A plot of $4\pi^2Dt$ versus t [where $t = (t_1 - t_0)$] for OBSL Phase V.

$$|C(k, t)| = |C_0| \exp[-\delta^2 k^2 / 2] \exp[-k^2 Dt]. \tag{21}$$

Thus

$$\ln |C(k, t)| = -\alpha(t)k^2 + \ln |C_0| \tag{22a}$$

with

$$\alpha(t) = \delta^2 / 2 + Dt. \tag{22b}$$

This is equivalent to the method of pairing the times as described in the previous section, but it is a little simpler numerically. Plots of $\ln |C(k, t_i)|$ versus k^2 for 16PC in DMPC and CSL in POPC are shown in Fig. 9 and Fig. 10. The time dependence of the slope of such plots, which gives D , is shown in Fig. 11 and Fig. 12 for the two phospholipid experiments.

As already mentioned, the liquid-crystal experiments were all performed at room temperature. However, the phospholipid experiments were carried out in a con-

TABLE I
Perpendicular Diffusion Coefficients
for Spin Probes in Phase V

Probe	Temp (K)	$D (\times 10^{-7} \text{ cm}^2 \text{ s}^{-1})$
TEMPONE	295	1.25 ± 0.12
OBSP	294	0.48 ± 0.13

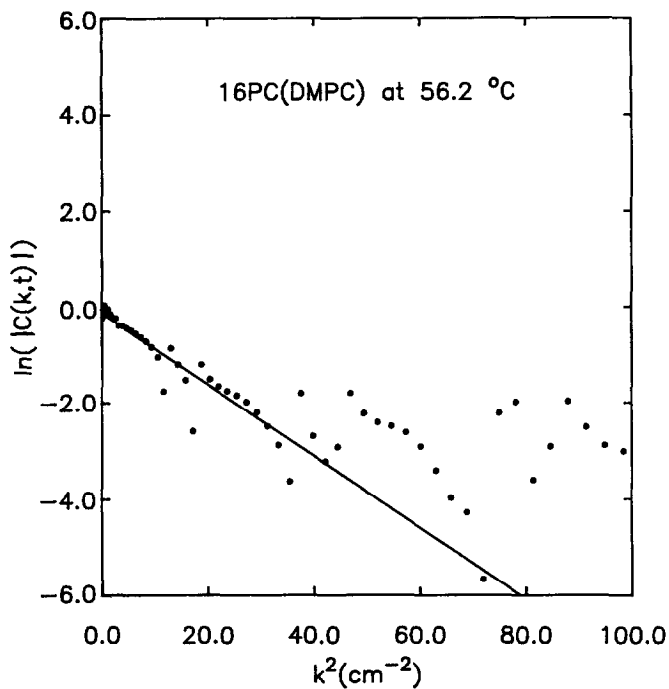


FIG. 9. A plot of $\ln|C(k)|$ versus k^2 for a particular time, t_i . The diffusing species is 16PC dissolved in DMPC. The slope of the line is proportional to $4\pi^2 D t_i$. [Note the scatter at $k^2 \approx 15$. This is due to nodes in $I_g(k)$ and $I_0(k)$ in this region, and such points are not included in the analysis.]

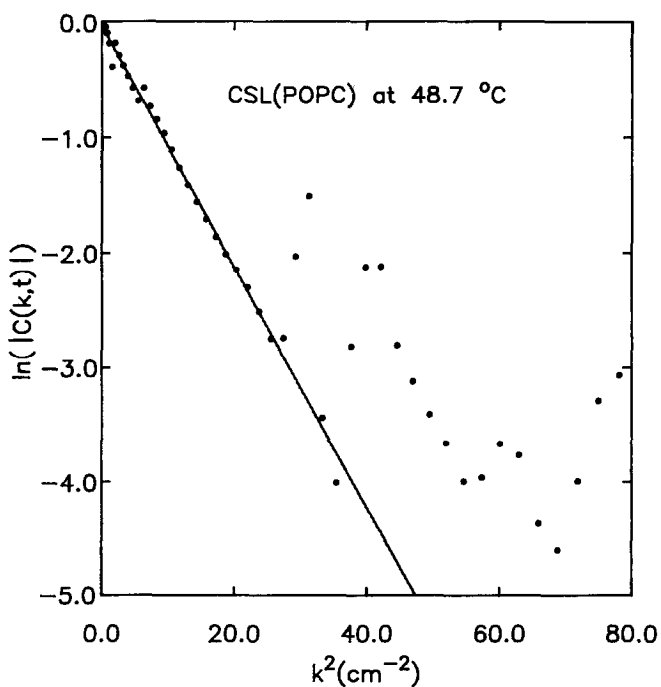


FIG. 10. Same type of plot as Fig. 9 except that the diffusing species is CSL in POPC.

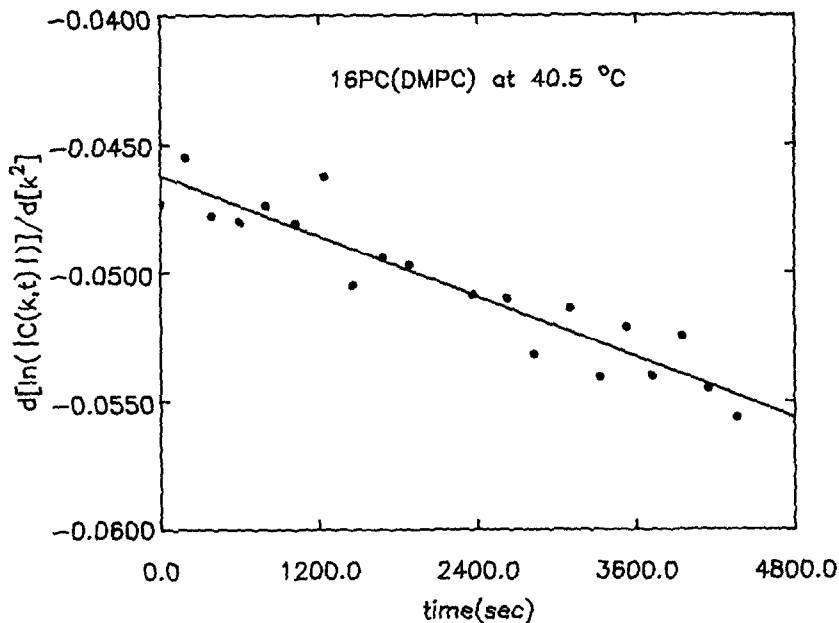


FIG. 11. A plot of the slopes calculated from a plot like that shown in Fig. 9 as a function of the times, t_i . The slope is equal to $-4\pi^2 D$. The diffusing species is 16PC in DMPC.

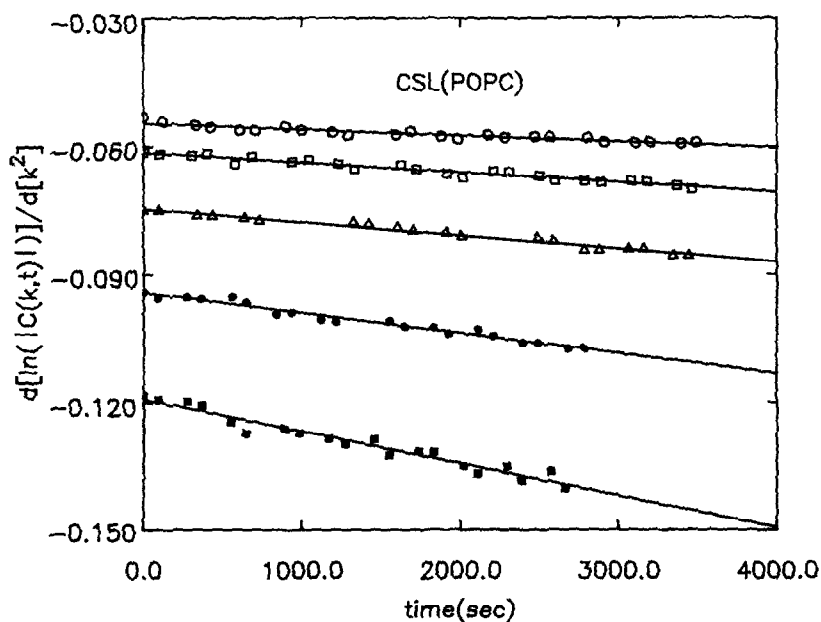


FIG. 12. Same type of plot as Fig. 11 except the diffusing species is CSL in POPC. The variation of D with temperature is also shown; 15.7°C (○), 25.3°C (□), 35.0°C (△), 48.7°C (●), and 63.0°C (■).

trolled-temperature Dewar. Therefore, plots of D versus temperature could be obtained as well as Arrhenius plots to determine the activation energy. Figures 13 and 14 are such Arrhenius plots. The values of D versus temperature for DMPC and POPC are listed in Tables 2 and 3. It should be noted that the magnitude ($10^{-8} \text{ cm}^2 \text{ s}^{-1}$) of D is one order smaller than we were able to report previously.

DISCUSSION

Liquid crystal. The two perpendicular diffusion coefficients obtained for the spin probes TEMPONE and OBSL in Phase V appear to be in a reasonable ratio. The perpendicular diffusion should be more sensitive than the parallel diffusion to the effect of probe length. The length of OBSL is two to three times longer than TEMPONE (see Fig. 15). We plan to study the parallel diffusion coefficients for these probes in subsequent work. As we pointed out earlier, a measurement of D (parallel) and D (perpendicular) for the isotropic phase of a solvent gives some indication of the reliability of the technique (7).

Phospholipids. The temperature dependence of D for the phospholipids was determined by using a single sample and recording spectra for approximately 1 h at a given temperature. Then the temperature was raised by about 10°C and another determination of D was made. This was done to avoid any possible effects of differences present in two samples prepared via the same procedure. The phospholipid samples are highly oriented, yet each sample contains a small amount of oily streak defects that is hard to control. The water content, which is 10–15% for these experiments, is also difficult to reproduce precisely. Water content has a significant influence on the rate

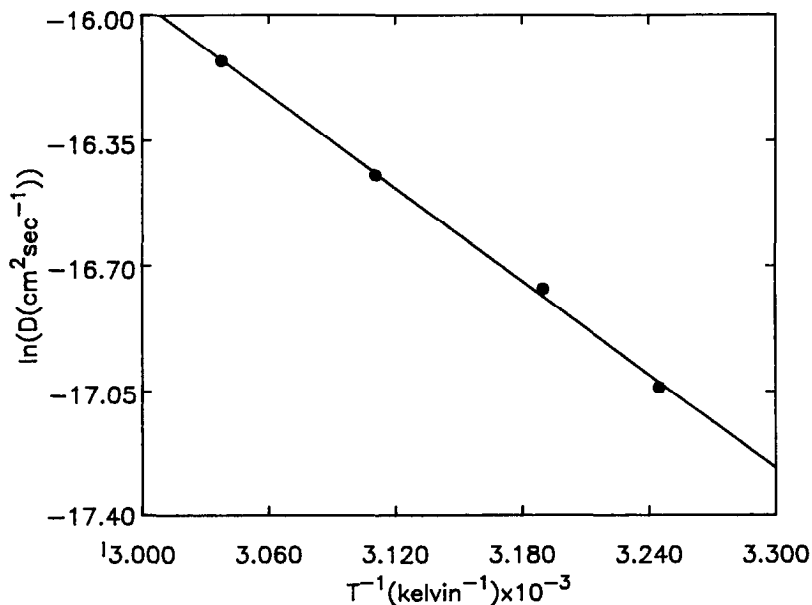


FIG. 13. Semi-log plot of data derived from Fig. 11 for 16PC in DMPC.

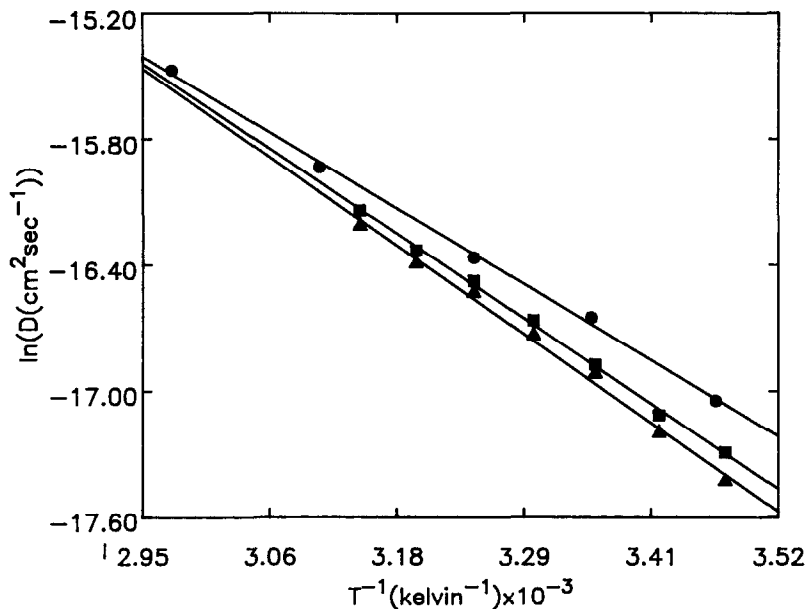


FIG. 14. Semi-log plots of diffusional data for various probes in POPC. The solid circles (●) are for CSL by ESR imaging from this work. The solid square boxes (■) and the solid triangles (▲) are, respectively, for NBD-DHPE and for NBD-DLPE from the FRAP experiments of Ref. (18).

of fast lateral diffusion in phospholipids, and this was another reason for using a single sample for a given series of temperature measurements.

The diffusion constants of CSL in POPC at various temperatures derived from our ESR imaging technique are very close to those of NBD-DHPE and NBD-DLPE as measured by the method of fluorescence recovery after photobleaching (FRAP) (18). The small differences may be due to the structural difference of probe molecules used in those two techniques. Semi-log plots of these data vs T^{-1} (Fig. 14) show non-Arrhenius type temperature dependence of diffusion constants in all cases. This plot also shows that CSL diffuses faster than NBD-DHPE and NBD-DLPE fluorescence probes in POPC at all temperatures.

General comments. The liquid-crystal work presented here served as a template for the development of the rapid determination technique. Other phases of liquid crys-

TABLE 2

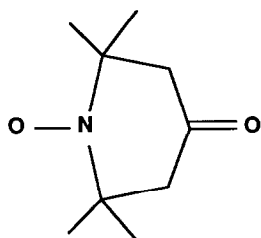
Lateral Diffusion Coefficient 16PC (DMPC)	
Temperature (°C)	$D (\times 10^{-8} \text{ cm}^2 \text{ s}^{-1})$
35.2	3.98 ± 0.56
40.5	5.24 ± 0.44
48.5	7.20 ± 1.16
56.2	9.90 ± 0.58

TABLE 3

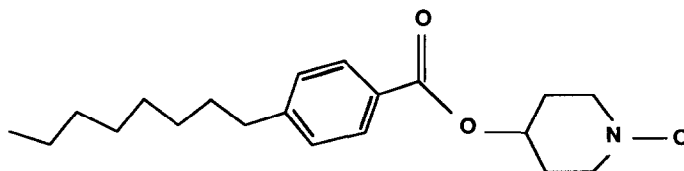
Lateral Diffusion Coefficients for CSL (POPC)	
Temperature (°C)	$D (\times 10^{-8} \text{ cm}^2 \text{ s}^{-1})$
15.7	3.96 ± 0.33
25.3	5.88 ± 0.30
35.0	7.82 ± 0.31
48.7	12.02 ± 0.51
63.0	19.09 ± 1.00

tals, such as the smectic phase, should in principle be amenable to investigation by the techniques outlined in this paper.

In studying diffusion in model membranes, the ESR imaging technique may have several advantages over the more commonly used methods, such as FRAP and excimer methods (18, 19). In general, the size of fluorescence active functional groups is much larger than ESR active nitroxide groups so that spin-labeled lipid molecules or cholesterol are structurally more similar to the parent molecule than an analogous fluorescence-labeled molecule. Thus, for biologically interesting molecules, such as cholesterol and the phospholipids themselves, it is conceivable that ESR imaging would result in more accurate estimates of the self-diffusion coefficients of unlabeled molecules. For example, with ESR imaging it is possible to study the diffusion of cholesterol and phospholipid independently in a phospholipid-cholesterol mixture of a model membrane, by utilizing cholestane probe for the cholesterol and spin-labeled phospholipid probes for the phospholipid. Moreover diffusion parallel to the



Tempone



Octylbenzoyl Spin Label (OBSL)

FIG. 15. Structures of TEMPONE and OBSL.

bilayer normal in oriented multilayers could be investigated (although it is generally much slower), provided a sample having an appropriate inhomogeneous spin-probe distribution can be made (20). One of the most distinct advantages of the ESR imaging method is that rotational diffusion, as well as translational diffusion, can be studied simultaneously. In the ESR imaging experiment, the usual ESR spectra, without any magnetic field gradient, also must be collected (see Experimental). By simulating those gradient-off spectra, rotational diffusion coefficients can be determined simultaneously with the translational diffusion coefficients. Of course this is also true for diamagnetic species studied by NMR methods (21), and for spin-labeled phospholipids studied by photobleaching ESR (22). For the photobleaching-ESR experiment, a photosensitive compound, such as an alkylcobalt complex, must be incorporated into the model membrane, and may affect the dynamics of phospholipid molecules.

The ESR imaging technique is a rapid one because the initial distribution of spin probes is confined to a small volume within the available solvent. The potential for rapid determination was proposed by us in our initial imaging paper (7). We speculated that a value of $D = 10^{-6} \text{ cm}^2 \text{ s}^{-1}$ could conceivably be determined in 10–15 h (down from 6 days), but that estimate turns out to be pessimistic by about a factor of 1000 (since we measure a $D = 10^{-8} \text{ cm}^2 \text{ s}^{-1}$ in about 1 h). Let us summarize the requirements for sensitivity and resolution in imaging of diffusion (7): (1) One should prepare samples with an initial concentration profile having a minimum half-width δ ; (2) then the gradient B' should be chosen so that $B' \cong \Delta/\delta$, where Δ is the half-width of a resolved hf line; (3) as the experiment proceeds one should reduce B' to its optimum: $B' \cong \Delta/(\delta^2 + Dt)^{1/2}$ if possible. The "resolution" in imaging can be written as $R \equiv \Delta/B'$ (23); thus (2) is equivalent to choosing B' so that $R = \delta$, emphasizing the importance of a narrow initial distribution. The actual resolution of a *diffusion* experiment is given by $\langle x^2 \rangle^{1/2}$, where $\langle x^2 \rangle = 2\Delta t D$ and Δt is the time required to obtain D . If, in time Δt , the initial width in the presence of the optimum initial gradient increases by a factor n , then $\Delta t = 2(n^2 - 1)\delta^2/D$, and $\langle x^2 \rangle^{1/2} = 2(n^2 - 1)^{1/2}\delta$ (7). Our analysis in k space is sensitive enough that it enables us to measure D for an $n \sim 1.05$, whereas $\delta \sim 0.2 \text{ mm}$ so that $\langle x^2 \rangle^{1/2} \sim 0.1 \text{ mm}$. This is actually close to our typical estimates from the experiments.

We now feel that determining the very small diffusion coefficient characteristics of polymers will be realized in the short term. An initial distribution of $1 \mu\text{m}$ of a spin probe with Δ of 1 G, a diffusion coefficient of $D = 10^{-12} \text{ cm}^2 \text{ s}^{-1}$, and a gradient of 3000 G/cm (24) should allow D to be determined in less than 10 h. The challenge of such an experiment is in the preparation of the initial distribution.

CONCLUSION

Rapid determination of diffusion coefficients using narrow initial distributions of spin probes and high magnetic field gradients has been demonstrated. The diffusion coefficient for TEMPONE (and OBSL) in Phase V was determined. Also, the lateral diffusion coefficients of CSL and 16PC were determined in DMPC and POPC. For the phospholipid, the activation energy for lateral diffusion was also determined.

REFERENCES

1. K. OHNO, *Jpn. J. Appl. Phys.* **23**, L224 (1984).
2. W. ZOMMERFELDS AND M. J. R. HOCH, *J. Magn. Reson.* **67**, 177 (1986).

3. E. G. JANZEN AND Y. KOTAKE, *J. Magn. Reson.* **69**, 567 (1986).
4. D. J. SLOOP, H.-L. YU, AND T.-S. LIN, *Chem. Phys. Lett.* **124**, 456 (1986).
5. G. R. EATON AND S. S. EATON, *J. Magn. Reson.* **71**, 271 (1987).
6. E. V. GALTSEVA, O. Y. YAKIMCHENKO, AND Y. S. LEBEDEV, *Chem. Phys. Lett.* **99**, 301 (1983).
7. J. P. HORNAK, J. K. MOSCIKI, D. J. SCHNEIDER, AND J. H. FREED, *J. Chem. Phys.* **84**, 3387 (1986); "Abstracts 7th International EPR Symposium, Rocky Mt. Conference, Denver, Colorado, August, 1984."
8. L. J. BERLINER AND H. FUJII, *J. Magn. Reson.* **69**, 68 (1986).
9. F. DEMSAR, P. CEVC, AND M. SCHARA, *J. Magn. Reson.* **69**, 258 (1986).
10. W. L. HUBBELL AND H. M. MCCONNELL, *J. Am. Chem. Soc.* **93**, 314 (1971).
11. H. TANAKA AND J. H. FREED, *J. Phys. Chem.* **88**, 6633 (1984).
12. R. N. BRACEWELL, "The Fourier Transform and Its Applications," 2nd ed. rev., p. 24, McGraw-Hill, New York, 1986.
13. J. CRANK, "The Mathematics of Diffusion," 2nd ed., p. 11, Oxford Univ. Press, Oxford, 1975.
14. P. M. MORSE AND H. FESHBACH, "Methods of Theoretical Physics," p. 862, McGraw-Hill, New York, 1953.
15. D. A. MCQUARRIE, "Statistical Mechanics," p. 386, Harper & Row, New York, 1976.
16. E. A. GUGGENHEIM, *Philos. Mag.* **2**, 538 (1926).
17. W. H. PRESS, B. P. FLANNERY, S. A. TEUKOLSKY, AND W. T. VETTERLING, "Numerical Recipes," p. 417, Cambridge Univ. Press, London/New York, 1986.
18. W. L. C. VAZ, R. M. CLEGG, AND P. HALLMAN, *Biochemistry* **24**, 781 (1985).
19. H. J. GALLA AND E. SACKMANN, *Biochim. Biophys. Acta* **339**, 101 (1974).
20. M. D. HOUSLAY, "Dynamics of Biological Membranes," p. 43, Wiley, Great Britain, 1982.
21. G. LINDBLOM, L. B. A. JOHNSON, AND G. ARVIDSON, *Biochemistry* **20**, 2204 (1981).
22. J. R. SHEATS AND H. M. MCCONNELL, *Proc. Natl. Acad. Sci. USA* **75**(10), 4661 (1978).
23. P. MANSFIELD AND P. G. MORRIS, "NMR Imaging in Biomedicine," p. 174, Academic Press, New York, 1982.
24. K. OHNO, "Abstracts 10th International EPR Symposium, Rocky Mt. Conference, Denver, Colorado, August, 1987."